

MICRO-MECHANICAL MODELLING OF DUCTILE TEARING RESULTING FROM A THERMO-MECHANICAL LOADING

M.P. Valeta¹, C. Poussard², F. Zydownik³ and C. Sainte Catherine⁴

¹ CEA, DRN/DMT/SEMT/LISN, 91191 Gif-sur-Yvette, France
Email : mpvaleta@cea.fr

² CEA, DRN/DMT/SEMI/LEMO, 91191 Gif-sur-Yvette, France
Email : christophe.poussard@drnsac.cea.fr

³ Ecole Centrale Nantes, 1 rue de la Noe, 44072 Nantes, France

⁴ CEA, DRN/DMT/SEMI/LCMI, 91191 Gif-sur-Yvette, France
Email : saintecatherine@drnsac.cea.fr

ABSTRACT

The Rousselier micro-mechanical model allows to account for the presence of voids in the matrix of the material which may coalesce and produce a crack when subjected to external mechanical loads or displacements. However, in some circumstances, thermal loads that result from plant operating conditions can not be neglected and have to be accounted for. The technical difficulty associated with this type of computation is to account for the dependence of the material stress strain curve with temperature. This was studied with the CEA finite element package CASTEM 2000 which includes a procedure that allows to interpolate linearly the stress strain curve of the material from a set of stress strain curves that have been obtained experimentally at different temperatures.

1. INTRODUCTION

The material selected for the study is a A508 ferritic steel for which tensile curves and J_R curves have been obtained for temperatures ranging between 5 to 300°C. The micro-mechanical damage parameters of the model are first identified for 3 temperatures by comparing the predicted experimental load versus diametrical reduction to experimental observations obtained from notched tensile specimens. This allows to verify that the initial void volume fraction is independent upon temperature. The model reproduces well the failure behaviour of the specimens for the 3 temperatures considered in the study provided that the temperature dependence of the stress strain curve is accounted for.

Then, the identified damage parameters are used to simulate ductile tearing in compact tension specimens (CT25) at different temperatures. The results obtained with the material stress strain curve at 150°C are compared with those obtained from the interpolated stress strain curve from the tensile curves at 5 and 300°C. The predictions are in good agreement with each other and compare favourably well with the experimental observations. The model allows to observe that increasing the operating temperature produces an increase of ductility which leads to an increase of the J_R curve, a diminution of the elastic slope on the load versus CMOD curve and a diminution of the maximum load bearing capacity of the specimen.

The practical interest of this investigation is then illustrated with two numerical simulations of ductile tearing that may result from the application of both an applied mechanical load and a thermal transient. Both an increasing and a decreasing thermal transient have been studied. The computations allow to observe a significant influence of the transients on the J_R curves : the increasing thermal transient produces a decrease of the initial J_R curve in comparison to the isothermal J_R curves. The initial slope of the J_R curve obtained with the decreasing thermal transient corresponds well to that obtained at the highest temperature but becomes closer to that obtained at 5°C as the temperature decreases.

2. IDENTIFICATION OF THE ROUSSELIER MODEL PARAMETERS FOR THE FERRITIC MATERIAL

The material considered in this investigation corresponds to the a ferritic steel (base material) used in the NESC [9] programme. The stress-strain curves determined at different temperatures are represented on Figure 1.

The Rousselier model [1] allows to predict the ductile fracture by introducing a damage parameter in the constitutive equation of the material :

$$F = \frac{\sigma_{eq}}{1-f} + D\sigma_1 f \exp\left(\frac{\sigma_m}{(1-f)\sigma_1}\right) - R(p)$$

$$1-f_0$$

where f is the void volume fraction, σ_{eq} the Von Mises stress, σ_m the hydrostatic stress and $R(p)$ the true stress-strain curve of the material. D is a constant often taken equal to 2 [2,3] and $\sigma_1 = 2/3*\sigma_{eq}$ [2,3] . Another parameter is usually employed, L_c , reflecting the statistical aspect of fracture and representing the average distance between inclusions present in the matrix of the material. L_c corresponds to the length of the finite element near the crack tip. So, several parameters need to be identified : the initial void volume fraction f_0 and the distance between the inclusions L_c .

First, the identification of f_0 has been realised using the experimental data available from notched tensile specimens (see Figure 2) with a radius of 2mm and 10mm at two temperatures : 25°C and 150°C. The identified value of f_0 must reproduce the initiation of a crack characterised on the tests results by a change of the slope after the instability. Figure 3 shows that the identified value ($f_0 = 3.10^{-3}$) allows to describe initiation at the 2 selected temperatures and is therefore temperature independent.

A similar approach is used to identify L_c : the experimental $J-\Delta a$ curve obtained on a CT25 with 20% of side-groove is compared to 2D finite element computations satisfying plane strain conditions with different L_c values. The mesh used for the calculations is shown in Figure 5. The results shown in Figure 4 demonstrate that the best correlation of the computations with the experimental data is obtained for $L_c = 0.2\text{mm}$.

3. GEOMETRICAL DATA AND LOADING

The aim of this study is to simulate ductile crack extension in a CT25 specimen submitted to an imposed load and a thermal transient. The geometry, the mesh (see Figure 5) and the finite element hypothesis are the same as used for the identification. The mechanical loading is an imposed displacement. Five thermal loadings have been computed and are summarised in the following tables.

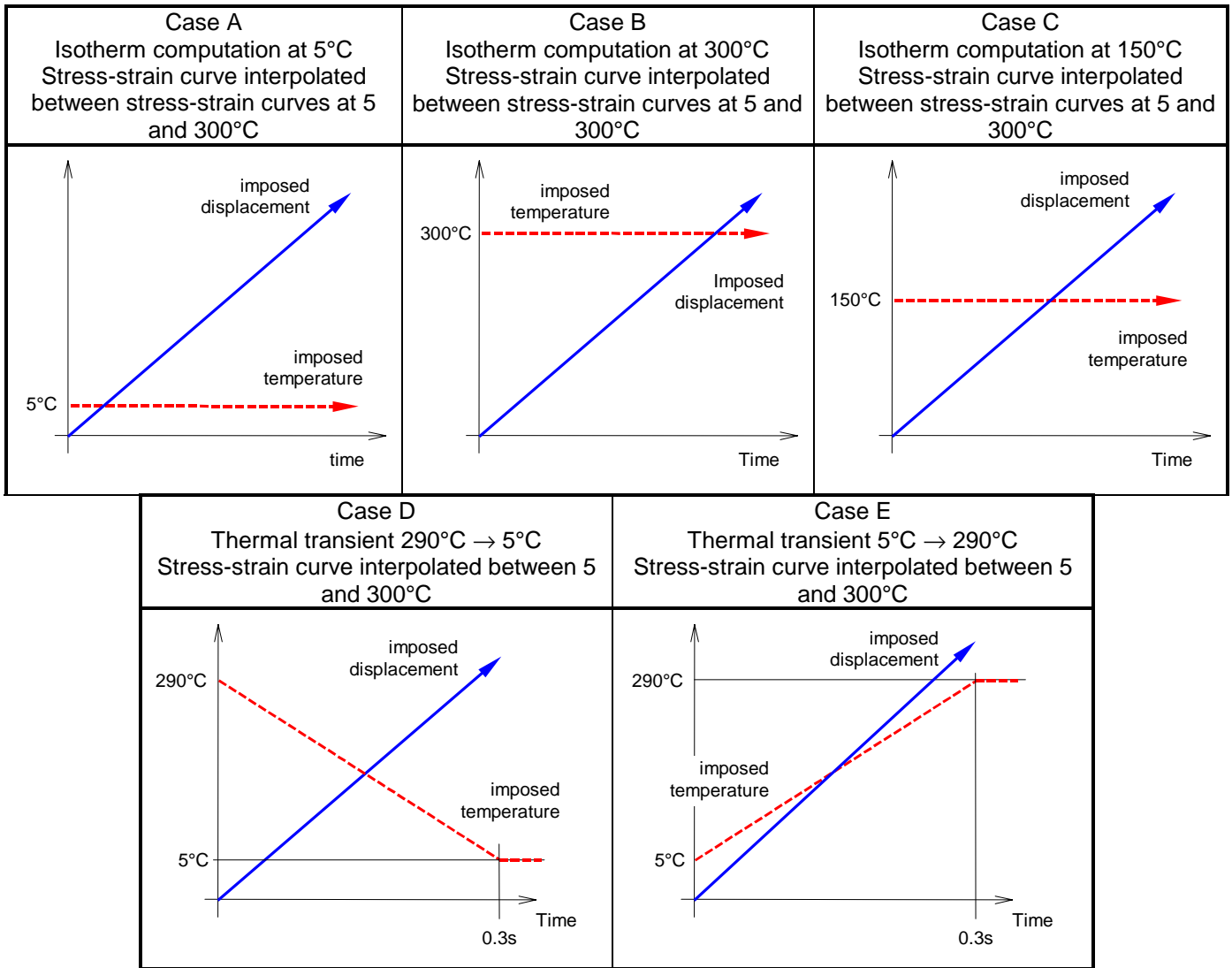


Table 1 : Thermal loadings

Cases A, B and C have been computed in order to validate the model. Then case D and E have been studied, the first one with an increasing temperature and the second one with a decreasing temperature. Case A and B will allow to surround the computational results of thermal transient. Case C will allow to find the same result as for the identification of L_C where the true stress-strain curve at 150°C has been used.

4. RESULTS

4.1 Isotherm computations

The finite element results obtained for the isotherm computations are presented on Figure 6 and Figure 7. On Figure 6, it can be observed that the curve obtained with the true stress-strain curve at 150°C (referred to as 'identification results') and the curve obtained for Case C are quite similar. Moreover the behaviour of the material at 150°C is bordered between the behaviour obtained at 5°C and 300°C. At high temperature, the material is ductile. This is the reason why the $J-\Delta a$ at 300°C is shifted up in comparison to that obtained at lower temperatures. At 5°C the material is less ductile. The lost of ductility does not involve a great difference on the $J-\Delta a$ in comparison to that at 150°C. The most important effect is shown on Figure 7 which represents the load versus CMOD. On this figure, material keeps a linear stiffness until 50kN instead of 25 kN at 300°C and 45 kN at 150°C. A pronounced increase of the instability load at 150°C in comparison with the behaviour obtained at 300°C can also be observed. It has to mentioned that the stress-strain curves between 5°C and 150°C are very close to each other in comparison to the stress-strain curve at

300°C (see Figure 1). It is therefore not surprising to observe important difference between the behaviour at 150°C and the behaviour at 300°C.

4.2 Thermal transient

The finite element results obtained for the thermal transient computations are presented on Figure 8 and Figure 9. One can see a real difference of behaviour in comparison to the results obtained with an isotherm loading. For case E where the temperature increases from 5°C to 290°C, the $J-\Delta a$ curve is higher than the case B where the temperature is remained constant at 300°C and the $\frac{dJ}{da}$ modulus increases with the crack propagation. This increase is due to the increase of ductility of the material during the loading which involve an increase of J value for a same crack propagation. For case D where the temperature decreases from 290°C to 5°C, numerical problems associated with the convergence appeared. The explains computation was ended at a crack propagation of about 0.7 mm. However, it can be observed that the $J-\Delta a$ curve for case D is lower than for isotherm cases.

Figure 9 shows that the initial behaviour of case E is close to the behaviour of case A and that the initial behaviour of case D is close to the behaviour of case B. From 0.8 mm of crack propagation, the curves cross and at the end, the behaviour of case E is close to case B and the behaviour of case D close to case A.

5. CONCLUSIONS

Crack propagation on CT25 specimen have been simulated with the Rousselier model as implemented in CASTEM2000. The purpose of these computations is to evaluate the ability of the model to account for the variability of the material stress-strain curve with temperature.

The first step was to identify the Rousselier model parameters at three different temperatures. During that step, it has been shown that the void volume fraction is temperature independent and that the identified Rousselier parameters allow to reproduce the behaviour of notched tensile specimen at 25°C and 150°C.

The second step allowed to check that the finite element results obtained with the material behaviour at 150°C and an interpolated stress strain curve with the behaviour at 5°C and 300°C are identical. The isotherm computations at 5°C and 300°C gave the expected results in comparison with the results obtained at 150°C : the increase of ductility with temperature lead to an increase of the $J-\Delta a$ curve, a decrease of the elastic slope on the load-CMOD curve and a decrease of the load at instability.

Then, the studies of two thermal transient showed that it is possible to simulate the specimen behaviour with a thermo-mechanical loading.

REFERENCES

- [1] Rousselier, G., 1986, *Les Modèles de Rupture Ductile et leurs Possibilités Actuelles dans le Cadre de l'Approche Locale*, EDF, Service Réacteurs Nucléaires et Echangeurs, Les Renardières, BP 1, F-77250, Moret-Sur-Loing, France.
- [2] Seidenfuss, M., 1992, *Untersuchungen zur Beschreibung des Versagensverhaltens mit Hilfe von Schädigungsmodellen am Beispiel des Werkstoffes 20 MnMoNi 5 5*, PhD Thesis, MPA Stuttgart, Germany.
- [3] Poussard, C., 1996, *Validation of the Rousselier Model on 2D FE Calculations of NT and CT Specimens with CASTEM 2000*, Rapport CEA DMT 96/283.
- [4] Poussard, C. and Seidenfuss, M., 1996, *ESIS TC8 Round Robin, Identification of the Rousselier Model Parameters for a 22 NiMoCr 3 7 Ferritic Steel with CASTEM 2000*, Rapport CEA DMT 96/379.
- [5] Poussard, C. and Sainte Catherine, C., 1998, *CEA Contribution to Phase II, Task A1 to the Numerical ESIS-TC8 Round Robin on Micro-Mechanical Models*, Rapport CEA DMT/SEMT/RT/98-035.

- [6] Poussard, C. and Sainte Catherine, C., 1998, *CEA Contribution to Phase II, Task A2 to the Numerical ESIS-TC8 Round Robin on Micro-Mechanical Models*, Rapport CEA DMT/SEMT/RT/98-037.
- [7] Poussard, C. and Seidenfuss, M., 1997, *On the Simulation of Ductile Crack Growth using the Rousselier Model*, Transaction of 14th Structural Mechanics In Reactor Technology Conference, SMIRT 14, GW/7, pp. 673-680, Lyon, France.
- [8] *CASTEM 2000*, 1996, Commissariat à l’Energie Atomique, DRN/DMT/SEMT/LAMS, F-91191, Gif-Sur-Yvette, France.
- [9] NESC DOC TG2 (96) 08, April 1998, *NESC1 Spinning Cylinder Test, Data Report of Material Characterisation Programme, Revision 2, Network for Evaluating Steel Components (NESC)*, Material task Group TG2.

APPENDIX

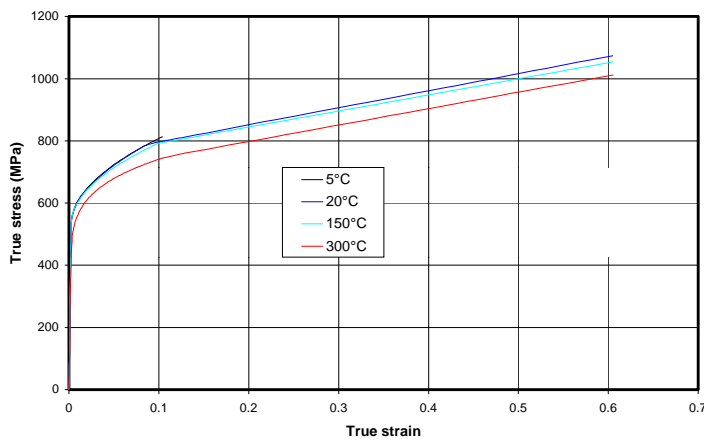


Figure 1 : True stress-strain curves

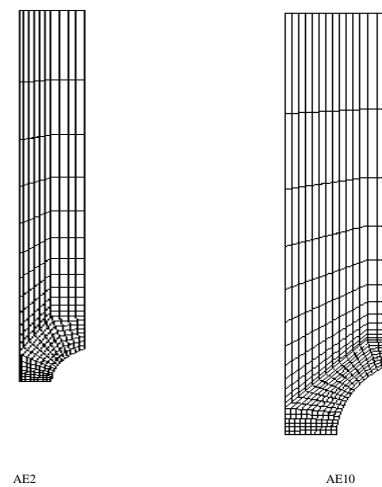
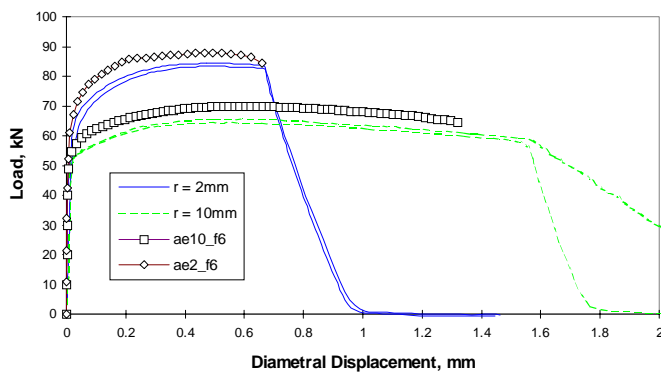
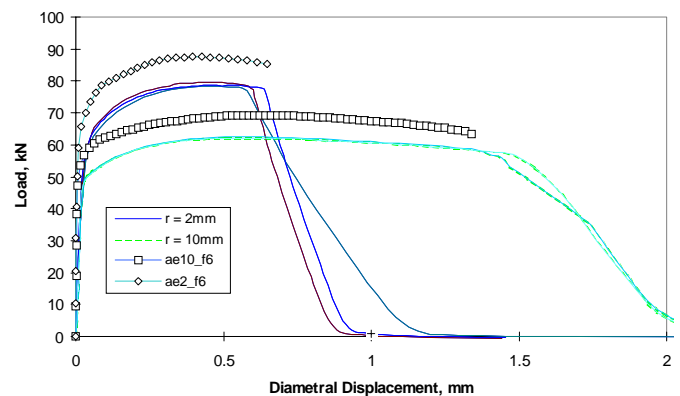


Figure 2 : Mesh of the notched tensile specimen



a)



b)

Figure 3 : Identification of f_0 at 25°C (a) and at 150°C (b)

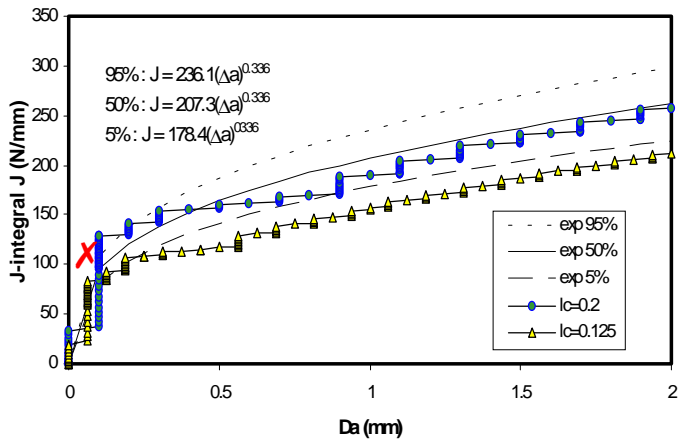


Figure 4 : Identification of L_C at 150°C

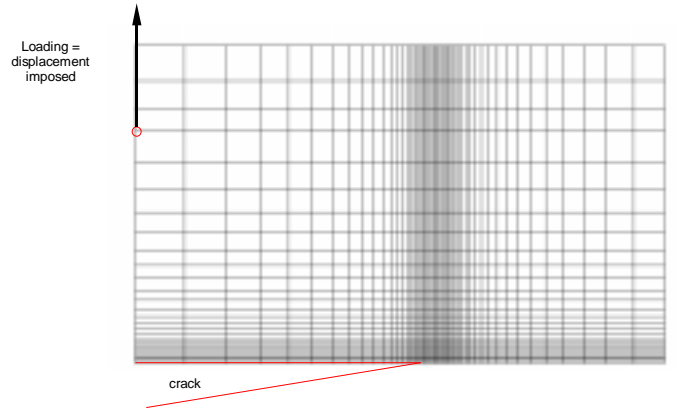


Figure 5 : Mesh of the CT25

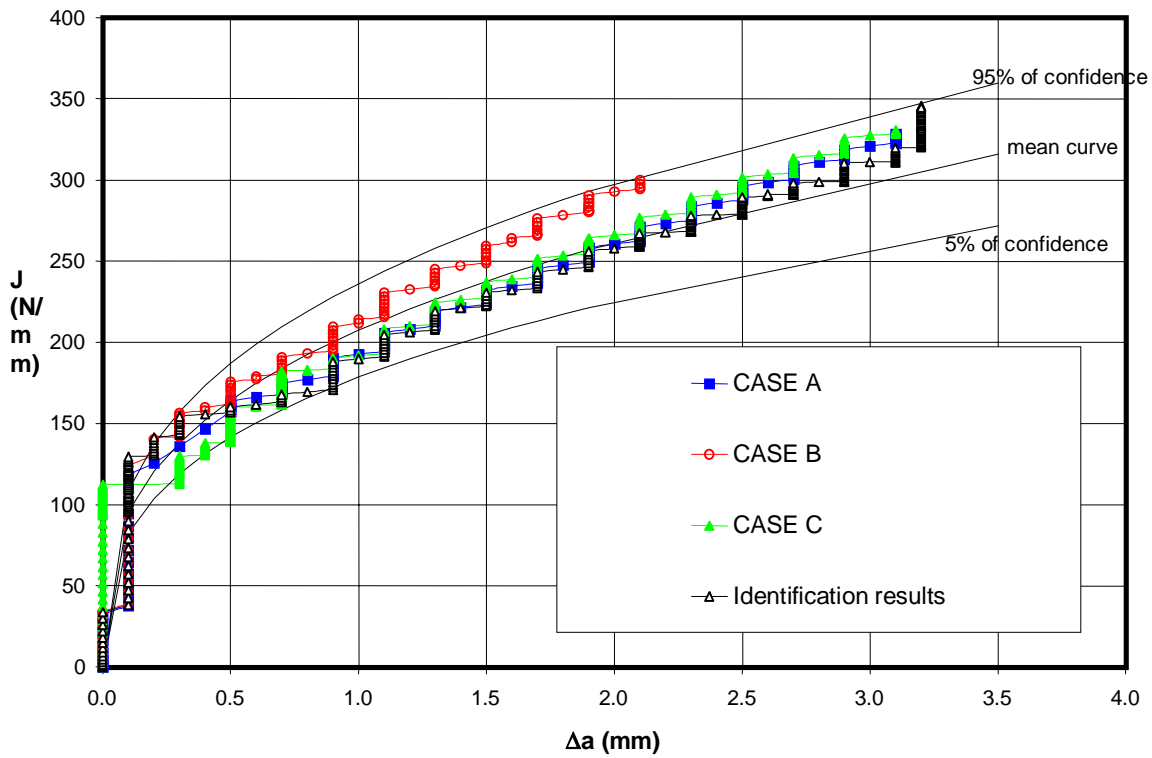


Figure 6 : $J-\Delta a$ curve for the cases A, B, C

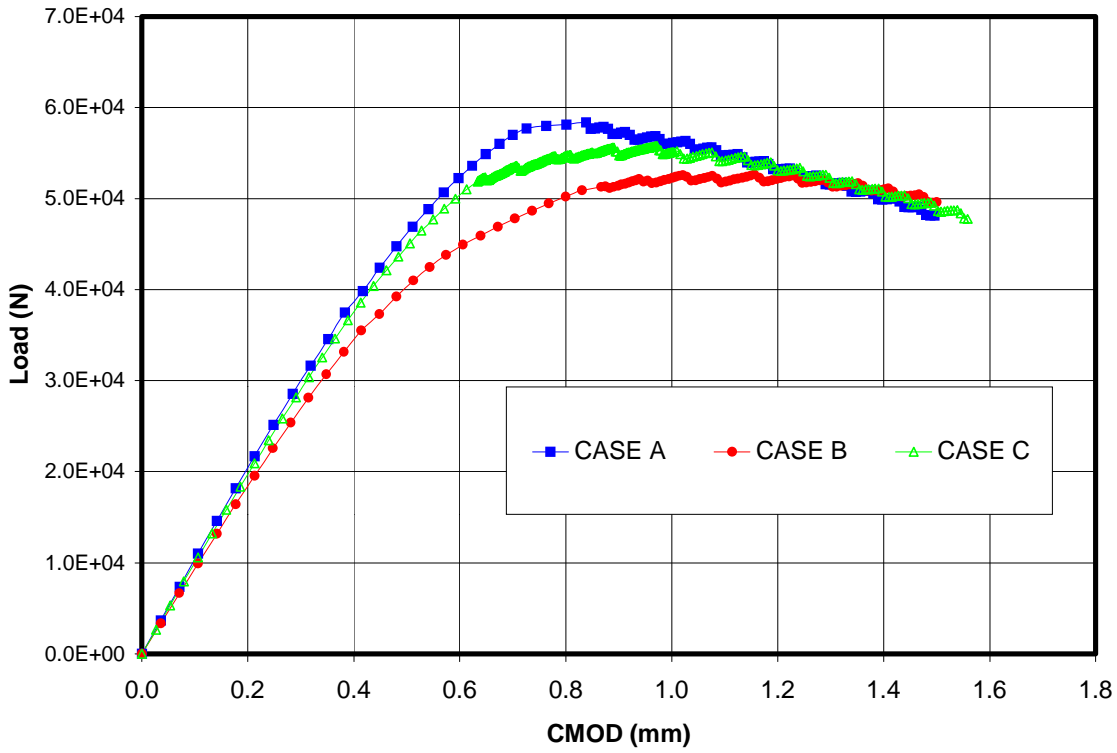


Figure 7 : Load versus CMOD for case A, B and C

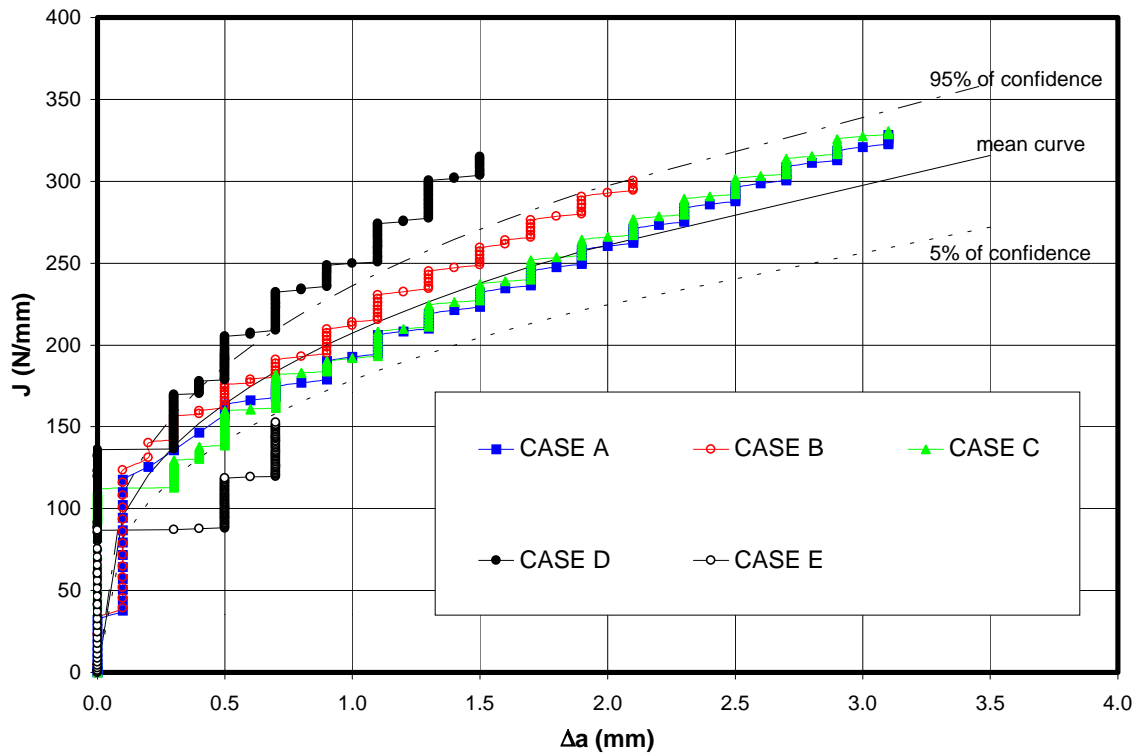


Figure 8 : J- Δa curve for the cases A, B, C, D and E

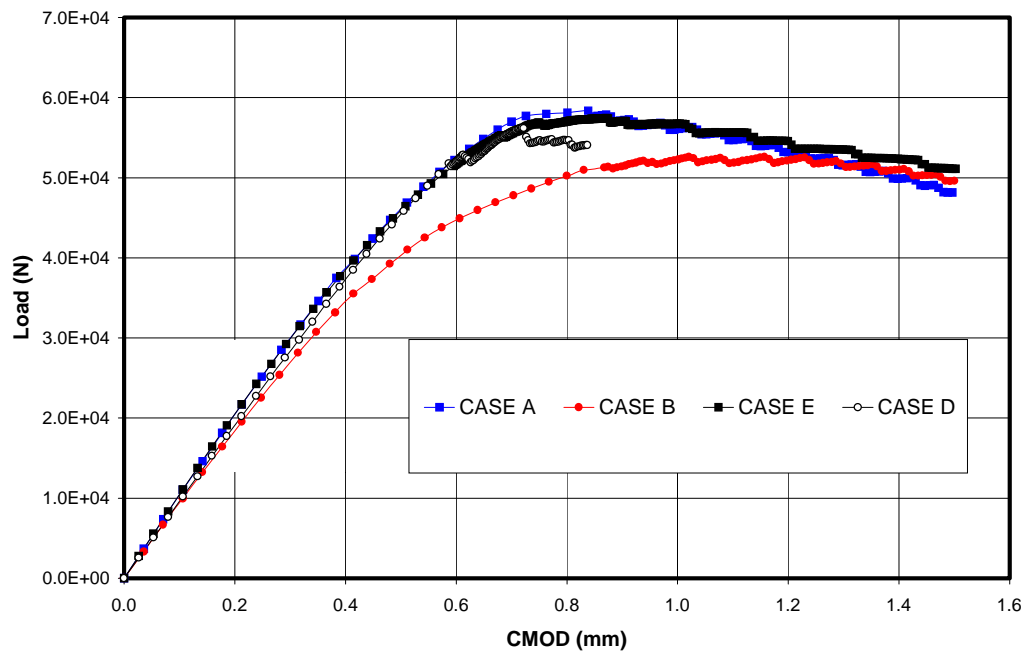


Figure 9 : Load versus CMOD for cases A, B, D and E